Title	Modeling radiated emissions through shielding boxes based on tangential electrical field samplings over openings
Author(s)	LI, P; Jiang, L
Citation	IEEE Transactions on Electromagnetic Compatibility, 2013, v. 55 n. 6, p. 1140-1146
Issued Date	2013
URL	http://hdl.handle.net/10722/185855
Rights	Creative Commons: Attribution 3.0 Hong Kong License

Modeling Radiated Emissions Through Shielding Boxes Based on the Tangential Electrical Field Samplings Over Openings

Ping Li, *Student Member, IEEE*, and Li Jun Jiang, *Senior Member, IEEE*

Abstract—The radiation from radiators such as PCBs inside an enclosed shielding box with ventilation slots is an important issue for electromagnetic compatibility or interference characterizations. In this paper, a two-step process is proposed based on the equivalence principle and the electric field integral equation method to complete the radiation prediction. The tangential electric fields over the slots on shielding boxes are first sampled to be the equivalent magnetic currents radiated from internal PCBs. In the second step, to avoid the computation of complex nonanalytical dyadic Green's functions when the field radiation is computed directly from the equivalent source, the surface current induced by the equivalent magnetic current is calculated by the method of moments. As a result, the total radiated emission is the superposition of both equivalent magnetic current source and induced current. To prove the validity and accuracy of the proposed approach, near-field and far-field radiations from PCBs in enclosed environments are benchmarked and compared with simulated references.

Index Terms—Dyadic green's function, equivalence principle, method of moments (MoM), perfect electrical conductor (PEC), planar electric near-field (NF) sampling, scattering issue, shielding box.

I. INTRODUCTION

USING numerical algorithms such as the finite-difference time-domain (FDTD) method, finite-element method (FEM), and method of moments (MoM) to directly solve electromagnetic compatibility (EMC) problems is becoming more challenging nowadays due to the ever increasing complexity of integrated circuits, printed circuit boards (PCB), and highly advanced packaging techniques [1]. The far-field (FF) measurement in the open area test site or semianechoic chambers is a broadly used technique in EMC to characterize the radiation behaviors of devices under test (DUT) at 3 and 10 m away from the DUT [2], [3]. Unfortunately, this method is time consuming and prohibitively expensive. To overcome these deficiencies, the near-field (NF) measurement and the followed NF-FF transformation algorithms are popular alternatives for the radiation

characterization [4]–[6]. Initially, researchers used these techniques for antenna radiation pattern characterizations, diagnostics, hot-spot identification, etc. Subsequently, this technique was also introduced to EMC/EMI studies.

The source reconstruction method (SRM) is another technique widely used to facilitate the NF-FF transformation. In [7]–[11], the equivalent currents are solved based on the measured or simulated NF data. These equivalent sources are distributed over a fictitious surface that can be a perfect electrical conductor (PEC), a perfect magnetic conductor (PMC) plane [7]–[8], an arbitrary closed surface [9], or the surface of the object itself [10]–[11]. Recently, SRM was directly applied to EMC purposes. The radiated emissions from PCBs are reproduced by equivalent sources. In [12]–[13], equivalent sources are a set of electric or magnetic dipoles while in [14] equivalent sources are represented by a set of pulse functions.

In this paper, we propose a radiation calculation method based on the field sampled over the slots opened on surfaces of the shielding box. Based on Schelkunoff's field equivalence principle [15], only tangential electric fields are sufficient to reproduce the external radiated field when the box's internal region is filled up with PEC. This is because the tangential magnetic fields corresponding to equivalent electrical currents have no contribution according to the reciprocity theorem. The tangential electric field serves as the equivalent magnetic current, but its radiation calculation is difficult because the dyadic Green's function (DGF) is particularly complex with the presence of a PEC box located in the free space. To overcome this issue, a two-step process is proposed: first, the tangential electric NFs are sampled (in our case, simulated data is employed) over the slots. They will be corresponding to the equivalent magnetic currents. Then, the surface current induced by these equivalent magnetic currents is obtained through MoM [16]. As a result, the total radiated emission is the superposition of the direct radiation from the equivalent magnetic current source and the scattered field from the induced current over the PEC box surface.

The organization of the rest paper is as follows: Section II will introduce the proposed two-step process approach; Section III investigates several benchmarks with simulated NF data to verify the proposed idea. Conclusions and discussions are presented at the end of this paper.

II. THEORY

PCBs are often placed inside highly conductive shielding boxes with ventilation slots. The radiation outside the box can be determined by the sampled tangential magnetic and electric
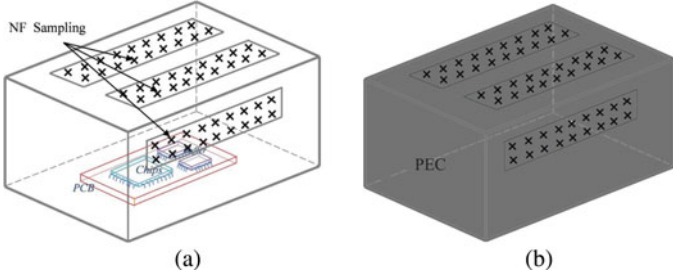
Fig. 1. (a) Geometry of a shielding box within electronic systems, and the setup of the planar NF sampling scenario. (b) Shielding box is filled with a PEC. The cross sign represents the field sampling position.

fields over the surface of the PEC shielding box. By the equivalence principle, only the tangential electric fields over slots are needed to characterize the external radiation properties when the internal box is filled with a PEC as shown in Fig. 1. It means only the tangential electric field sampling is needed over the slot apertures while the magnetic field sampling is not required. The electric and magnetic fields originated from the equivalent magnetic current are formulated as follows [20]:

$$\mathbf{E}(\mathbf{r}) = \int_{\text{slots}} \nabla \times \overline{\overline{\mathbf{G}}}_{\text{PEC}}(\mathbf{r}, \mathbf{r}') \cdot [\hat{\mathbf{n}}' \times \mathbf{E}(\mathbf{r}')] dS' \quad (1)$$

$$\mathbf{H}(\mathbf{r}) = -\int_{\text{slots}} i\omega\epsilon \overline{\overline{\mathbf{G}}}_{\text{PEC}}(\mathbf{r}, \mathbf{r}') \cdot [\hat{\mathbf{n}}' \times \mathbf{E}(\mathbf{r}')] dS' \quad (2)$$

where $\overline{\overline{\mathbf{G}}}_{\text{PEC}}$ is the DGF with the presence of the PEC box, $\mathbf{E}(\mathbf{r}')$ is the sampled tangential electric field over the slots, $\hat{\mathbf{n}}'$ is the unit normal vector over slot surfaces, and $-\hat{\mathbf{n}}' \times \mathbf{E}(\mathbf{r}')$ corresponds to the equivalent magnetic current. Because the closed form solution of the DGF in (1) is not available due to the presence of a PEC box, it is difficult to compute the radiated field based on the equivalent magnetic current. One approach is to use algorithms like MoM to numerically compute the DGF. But it is very time consuming [18], [21].

In this paper, the following two-step process is proposed to avoid the computation of this complex DGF. First, the equivalent magnetic current is sampled to be the excitation source. To obtain its radiation, we actually compute the radiation from both equivalent magnetic and its induced currents on the surface of the PEC box. If $\mathbf{E}(\mathbf{r})$ is the total radiated field. It can be written as [16]

$$\mathbf{E}(\mathbf{r}) = \mathbf{E}_{\text{inc}}(\mathbf{r}) + \mathbf{E}_{\text{sca}}(\mathbf{r}). \quad (3)$$

The first term at the right-hand side of (3) is the free-space field originated from the equivalent magnetic current, it can be calculated by

$$\mathbf{E}_{\text{inc}}(\mathbf{r}) = \int_{S'} \nabla \times \overline{\overline{\mathbf{G}}}(\mathbf{r}, \mathbf{r}') \cdot [\hat{\mathbf{n}}' \times \mathbf{E}(\mathbf{r}')] dS' \quad (4)$$

where

$$\overline{\overline{\mathbf{G}}} = \left(\overline{\overline{\mathbf{I}}} + \frac{\nabla \nabla}{k^2} \right) \frac{e^{ik|\mathbf{r} - \mathbf{r}'|}}{4\pi|\mathbf{r} - \mathbf{r}'|} \quad (5)$$

is the free space DGF. S' denotes the surface where slots reside. The second term on the right-hand side of (3) is the scattered

field generated from the induced current

$$\mathbf{E}_{\text{sca}}(\mathbf{r}) = i\omega\mu \int_S \overline{\overline{\mathbf{G}}}(\mathbf{r}, \mathbf{r}') \cdot \mathbf{J}_s(\mathbf{r}') dS' \quad (6)$$

where $\mathbf{J}_s(\mathbf{r}')$ is the induced current over the surface of the PEC box. S denotes all external surfaces of the shield box.

At the second step, we need to determine the induced electric current on the PEC surface excited by the equivalent magnetic current. By employing the PEC boundary condition $\hat{\mathbf{n}} \times \mathbf{E} = 0$ and substituting (6) and (4) into (3), we have

$$-\hat{\mathbf{n}} \times \mathbf{E}_{\text{inc}}(\mathbf{r}) = i\omega\mu \int_{S'} \hat{\mathbf{n}} \times \overline{\overline{\mathbf{G}}}(\mathbf{r}, \mathbf{r}') \cdot \mathbf{J}_s(\mathbf{r}') dS. \quad (7)$$

Then the Rao–Wilton–Glisson (RWG) basis function [17] is used to approximate the unknown induced electric current:

$$\mathbf{J}_{s'}(\mathbf{r}') = \sum_{n=1}^{N} I_n \mathbf{J}_n(\mathbf{r}') \quad (8)$$

where $\mathbf{J}_n(\mathbf{r}')$ is the nth RWG basis, N is the total number of basis functions, and I_n is its coefficient to be calculated. Substituting (8) into (7), testing it by $-\hat{\mathbf{n}} \times \mathbf{J}_m(\mathbf{r}')$ with $m = 1, \ldots, N$, and then integrating the resultant dot product over the surface of the PEC cube scatter, we have

$$-\int_S \mathbf{J}_m(\mathbf{r}) \cdot \mathbf{E}_{\text{inc}}(\mathbf{r}) dr$$

$$= i\omega\mu \sum_{n=1}^{N} \int_S dr \mathbf{J}_m(\mathbf{r}) \cdot$$

$$\int_S \overline{\overline{\mathbf{G}}}(\mathbf{r}, \mathbf{r}') \cdot \mathbf{J}_n(\mathbf{r}') dr' \quad m = 1, \ldots, N. \quad (9)$$

We write (9) as an MoM matrix equation

$$\overline{\mathbf{V}}_m = \overline{\overline{\mathbf{Z}}}_{mn} \overline{\mathbf{I}}$$

$$m = 1, \ldots, N; \quad n = 1, \ldots, N \quad (10)$$

where $\overline{\overline{\mathbf{Z}}}_{mn}$ is the impedance matrix with

$$Z_{mn} = i\omega\mu \langle \mathbf{J}_m, \overline{\overline{\mathbf{G}}}, \mathbf{J}_n \rangle \quad (11)$$

and $\overline{\mathbf{V}}_m$ is the excitation vector with

$$V_m = -\langle \mathbf{J}_m, \mathbf{E}_{\text{inc}} \rangle \quad (12)$$

where $<,>$ means the inner product defined as

$$<\phi, \psi> = \int_S \phi \cdot \psi dr. \quad (13)$$

To solve the square matrix equation system (10), an iterative process generalized minimum residual (GMRES) method is applied.

After finding out the induced current, the total radiation from the equivalent magnetic current is conveniently obtained by (3) with both (4) and (6).

III. NUMERICAL RESULTS

In this section, several numerical examples are investigated to verify the accuracy and feasibility of the proposed approach. In
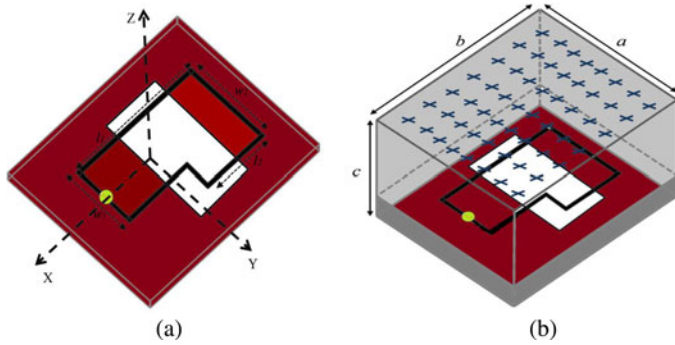
Fig. 2.   (a) Physical layout of the analyzed PCB ($l_1 = 80$ mm, $l_2 = 38.5$ mm, $W_1 = 20$ mm, and $W_2 = 40$ mm). (b) Geometrical structure of the shielding cavity and the planar NF measurement scenario ($a = 140$ mm, $b = 140$ mm, and $c = 100$ mm).

order to test and validate NF-FF transformation algorithm, synthetic data are often preferred because the accuracy of the data is easy to be controlled and compared to the real measurements. Also, particular error effects and measurement influences can be incorporated into the synthetic data to check the robustness of the proposed method. Hence, to benchmark our methodology flexibly, the synthetic NF data are obtained by the simulated data from the commercial full-wave solver FEKO that is based on MoM [16]. Apart from the FF comparison, the transformed field data over certain planes in the NF region are also compared with those from the simulations using FEKO [19].

A. PCB With a Loop Transmission Line Over a Slot Placed in a Rectangular PEC Cavity Without the Shielding Cover on the Top Surface

A loop transmission line on a PCB with the characteristic impedance $Z_0 = 50$ Ω is driven by a 1 V radio frequency (RF) voltage source operating at 100 MHz, as shown in Fig. 2(a). It is placed in a PEC shielding box with the shielding cover removed. To investigate its radiation behavior, the NF over the top box aperture plane is sampled as shown in Fig. 2(b). The sampled data are actually obtained from the FEKO simulation. Then, the sampled tangential field is applied to the proposed two-step process to complete the NF-FF transformation. In this example, the tangential components E_x and E_y are sampled with spatial resolution $\Delta x = \Delta y = 1$ cm. The sampling resolution along x and y directions depends on the numerical discretization on the right-hand side of (4) and the accuracy requirement on the left-hand side of (9). Also, depending on the operating frequency, the field variation over the slot could change significantly. Hence, the sampling density has to meet certain criteria to guarantee a reliable recovery of the radiated field from slots. Because the field is truncated, high-order Gaussian quadrature rules can be used to decide the exact position of the sampling points. But for convenience purposes, uniform distance sampling is actually preferred since the quadrature point positions are not always equally spaced. Normally, the density of samples shall not be larger than 1/10th of the wavelength.

To show the accuracy of our method, the radiated electric fields over two concentric spherical surface with radii $R = 3$ and 10 m are calculated and compared with numerical simulations
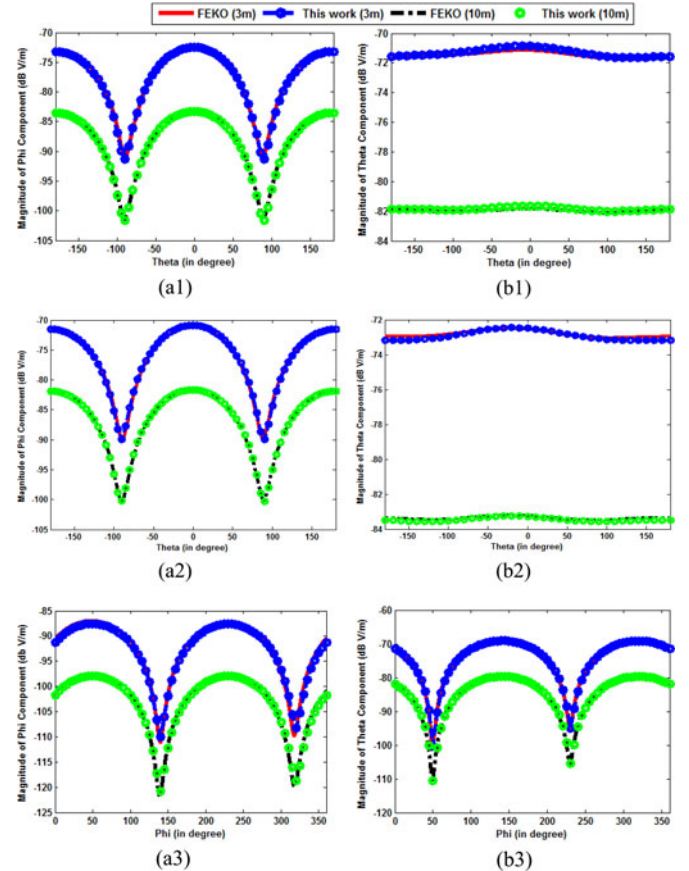

Fig. 3.   Calculated electric fields at 3 and 10 m for benchmark A. The left column are the ϕ-components, and the right column are the θ-components. (a1 and b1) E-field in the xoz plane. (a2 and b2) E-field in the yoz plane. (a3 and b3) E-field in the xoy plane.

by FEKO, as shown in Fig. 3. It can be seen that excellent agreements are achieved in both vertical and horizontal cutting planes. The deep nulls are also captured by the proposed two-step process approach.

The proposed method is also effective for NF-NF transformations. Such kinds of techniques are quite useful for source diagnostics and hot-spot identifications in PCBs. To examine the accuracy of this approach, the electric NFs have been calculated in the plane $z = 0.15$ m and $z = 0.3$ m. The dimensions of these two planes are 0.4 m in both x and y-directions. The 3-D field distribution is shown in Fig. 4. The reference solutions are also presented.

B. PCB With an L-Shape Transmission Line in a Rectangular PEC Cavity With Five Slots Distributed on Surfaces

In the second benchmark, a closed PEC box is employed. For heat ventilation purposes, ventilation slots are opened on the box, as shown in Fig. 5. A PCB with an L-shape transmission line is placed inside this closed box and driven by an RF voltage source operating at 1 GHz. The synthetic NF data over the five slots are generated from the FEKO simulation. During the iterative GMRES MOM process, the convergence rate of the proposed approach versus the iteration number is presented in
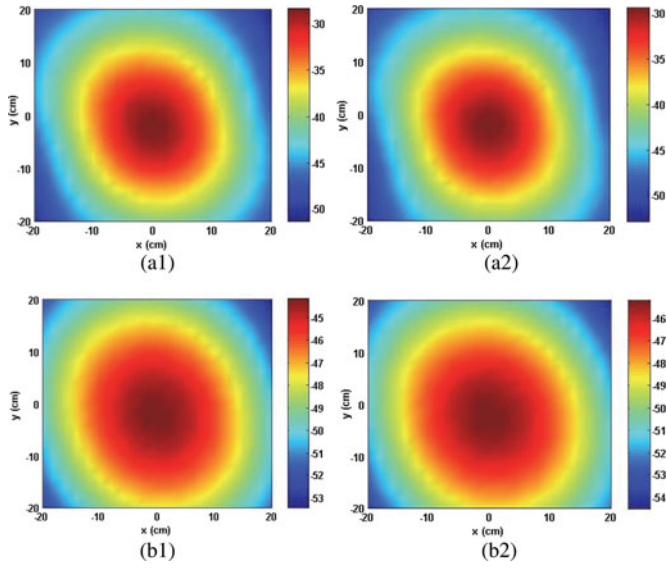
Fig. 4. (a1) Total electric field (dB·V/m) in the plane $z = 0.15$ m calculated from the proposed method. (a2) Reference result by FEKO simulation. (b1) Total electric field (dB·V/m) in the plane $z = 0.3$ m calculated from the proposed method. (b2) Reference result by FEKO simulation.
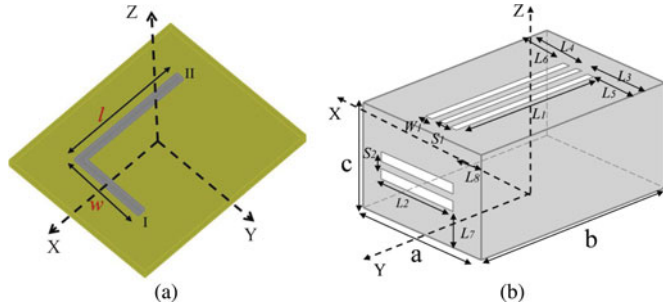

Fig. 5. (a) Physical layout of the PCBs ($l = 100$ mm, $w = 70$ mm). (b) Geometrical outline of the PEC shielding cavity ($a = 140$ mm, $b = 140$ mm, $c = 100$ mm, $l_1 = 100$ mm, $l_2 = 100$ mm, $l_3 = 60$ mm, $l_4 = 60$ mm, $l_5 = 20$ mm, $l_6 = 20$ mm, $l_7 = 30$ mm, $S_1 = 10$ mm, $S_2 = 10$ mm, and $W_1 = 20$ mm).
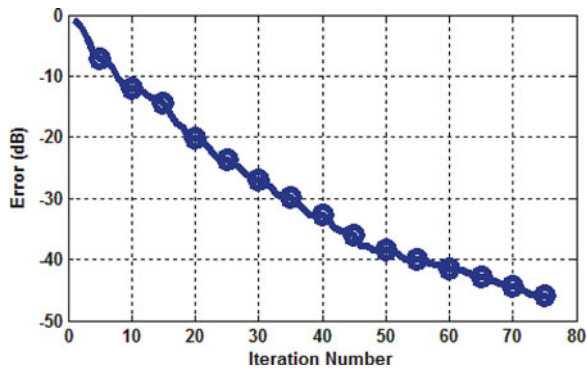

Fig. 6. Convergence rate of the proposed algorithm versus the iteration number for benchmark B.

Fig. 6. In our case, the error criterion is 0.5%. To achieve this criterion, the corresponding iteration number is 75.

For the radiated field predication, as seen from Fig. 7, the θ- and ϕ-components of electric fields over a spherical surface of radius $R = 3$ m calculated by the proposed method fit very well
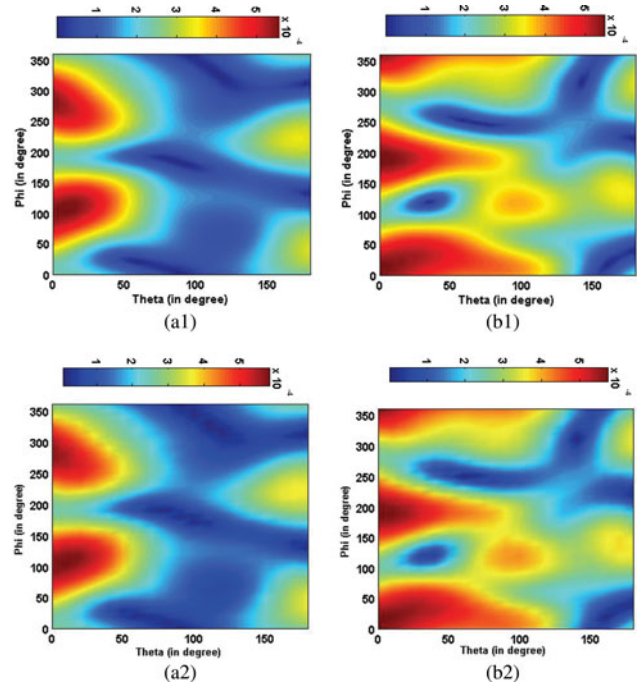

Fig. 7. Electric field (V/m) over a sphere with radius $R = 3$ m: the first row is calculated by the proposed approach, the second row is calculated by FEKO. (a1 and a2) Amplitude of E_ϕ. (b1 and b2) Amplitude of E_θ.

with those simulated by FEKO. To further verify the accuracy of the proposed method, the transformed fields at different cut planes are plotted in Fig. 8. Also, good agreements are observed. There are small discrepancies for E_ϕ in the deep nulls of the vertical plane around $\phi = \pm 90°$ in Fig. 8(a1) and the horizontal plane around $\phi = 0°$ and $185°$ in Fig. 8(c1). This is due to the numerical error in capturing higher order modes, which will be discussed in Section III-C. The accuracy of the proposed method is further verified by the similarity between the predicted NF and the simulated ones by FEKO. To show the capability of capturing evanescent waves in the proposed method, the NFs over planes located at $z = 0.3$ m and $y = 0.4$ m with square dimensions 0.6 m $\times 0.6$ m are calculated. The results are shown in Fig. 9. Good agreements are noted, although their similarities are not as good as the FF radiation. This is due to the fact that NFs are more sensitive to numerical errors due to the existence of high-order modes.

To have a quantitative comprehension of the accuracy of the proposed transformation algorithm, the following mean squared error (MSE) function is employed as the error indicator [11], [13], [22].

$$\sigma_{\mathrm{MSE}} = 10\log_{10} \frac{\sum |\mathbf{E}^{\mathrm{ref}}(r, \theta, \phi) - \mathbf{E}^{\mathrm{new}}(r, \theta, \phi)|^2}{\sum |\mathbf{E}^{\mathrm{ref}}(r, \theta, \phi)|^2} \quad (14)$$

where $\mathbf{E}^{\mathrm{ref}}$ is the actual tangential field calculated by FEKO, $\mathbf{E}^{\mathrm{new}}$ is the the tangential field calculated by the proposed method, and (r, θ, ϕ) is the spherical coordinate. Both $\mathbf{E}^{\mathrm{ref}}$ and $\mathbf{E}^{\mathrm{new}}$ are sampled on a series of concentric spherical surfaces.

The error indicator in (14) is presented as a function of the observation distance from the DUT as shown in Fig. 10. It can be seen that the error decreases with the increasing observation
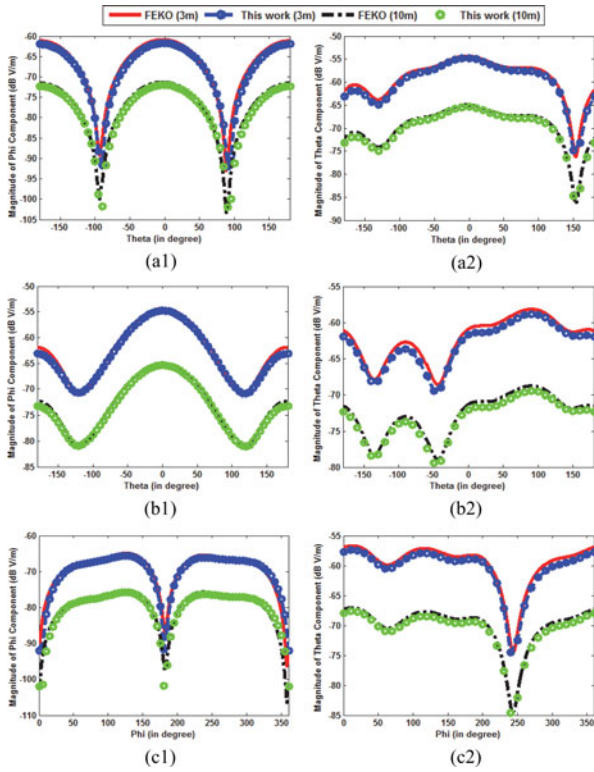
Fig. 8. Calculated electric fields at 3and 10 m for benchmark B. The left column is for the ϕ-components, the right column is for the θ-components. (a1and a2) E-field in the xoz plane. (b1and b2) E-field in the yoz plane. (c1and c2) E-field in the xoy plane.
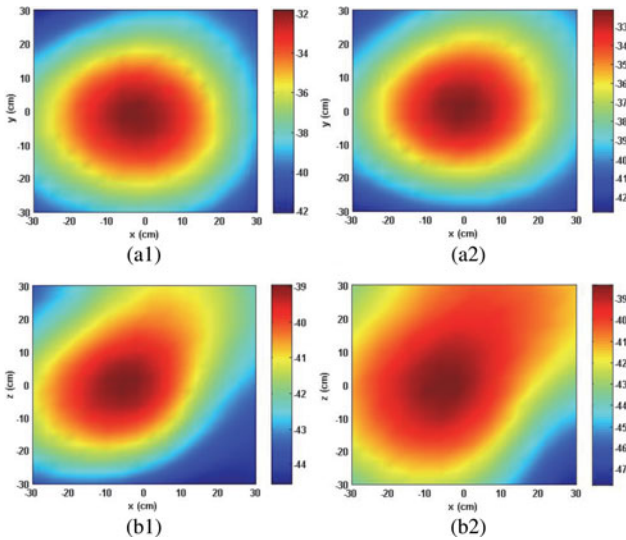

Fig. 9. (a1) Total electric field (in dB·V/m) at the plane $z = 0.3$ m calculated from the proposed method. (a2) Reference result by FEKO simulation. (b1) Total electric field at the plane $y = 0.4$ m calculated from the proposed method. (b2) Reference result by FEKO simulation.

distance. This is reasonable since the field distribution in the NF field region is quite complex due to the existence of evanescent waves.
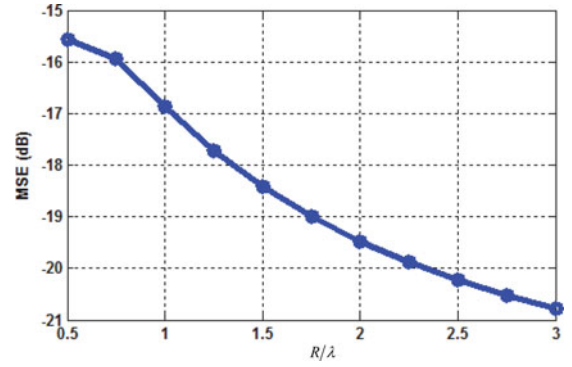

Fig. 10. Mean-squared error function MSE (in dB) versus the observation distance (the radius of the testing spherical surface).
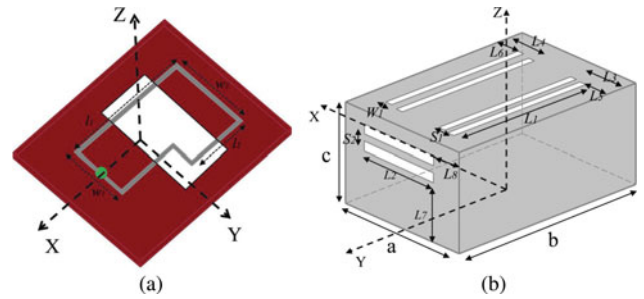

Fig. 11. (a) Physical layout of the PCBs. (b) Geometry of the PEC shielding cavity ($a = 140$ mm, $b = 140$ mm, $c = 100$ mm, $l_1 = 100$ mm, $l_2 = 100$ mm, $l_3 = 40$ mm, $l_4 = 40$ mm, $l_5 = 20$ mm, $l_6 = 20$ mm, $l_7 = 50$ mm, $l_8 = 20$ mm, $W_1 = 10$ mm, $S_1 = 10$ mm, and $S_2 = 10$ mm).
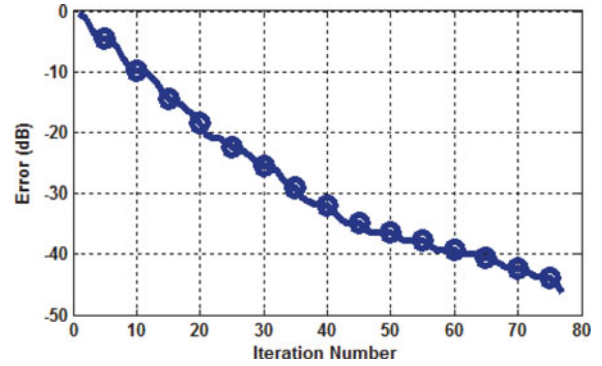

Fig. 12. Convergence rate of the proposed algorithm versus the iteration number for benchmark C.

C. PCBs With a Loop Transmission Line Over a Slot Placed in a Rectangular PEC Cavity With Six Ventilation Slots on the Surface of the Shielding Box

The PCB with the same physical layout as mentioned in Section III-A is placed in a closed PEC shielding box with six heat ventilation slots as shown in Fig. 11. It is driven by a 1 GHz voltage source. Again, the sampled electric fields over the six slots are generated from the FEKO simulation. By applying the proposed two-step method, the convergence property of the MOM process (second process) for this problem is obtained and shown in Fig. 12.

To have a better insight to the accuracy of our method, the amplitude of the radiated electric field over a spherical surface with
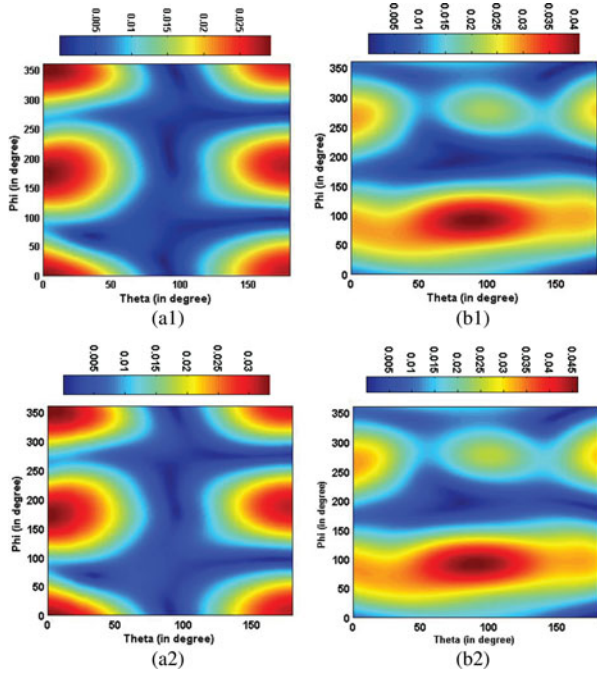
Fig. 13. Electric field (V/m) over a sphere with radius $R = 3$ m: the first row calculated by the proposed approach, the second row calculated by FEKO. (a1and a2) Amplitude of E_ϕ. (b1and b2) TAmplitude of E_θ.

$R = 3$ m is shown in Fig. 13. Excellent agreements are observed. Fig. 14 shows the dominant electric field components in the vertical and horizontal cutting planes of the two concentric spheres with radii $R = 3$ and 10 m, respectively. There are some discrepancies happening at the deep nulls for the ϕ component and the θ component. These discrepancies are mainly attributable to the higher order modes. There are high-order mode fields at the surfaces of slots and the high-order mode currents excited by the slots. They all generate radiations, and evanescent waves of higher order modes will attenuate more quickly. To make the algorithm more accurate, more modes need to be captured. It requires finer mesh over the PEC surface and dense sampling over slots.

To further study the accuracy and reliability of the proposed NF-NF or NF-FF transformation method, the MSE in (14) is employed as a function of the distance from the DUT again. The amplitude of the tangential electric components is calculated over a set of concentric spherical surfaces with radii from 0.5λ to 3λ. The results are shown in Fig. 15. As can be seen, the error is degrading with the increasing observation distance. It means that the NF radiation is more difficult to be captured than the FF due to those evanescent high-order modes.

The imperfections in the real measurement environment, such as cable influences, positioning errors, reflections from the side absorbing walls, and probe error, could affect the accuracy of the radiated field evaluation. Hence, noise contaminated electric field data are employed to study this issue. Uncorrelated complex white Gaussian noise regularized by signal-to-noise ratio (SNR) is added to the simulated noise-free data. To have a better understanding of its influence, MSE in (14) is employed as the indicator, again. The results are shown in Fig. 16. The results indicate that the noise 20 dB lower than the measured
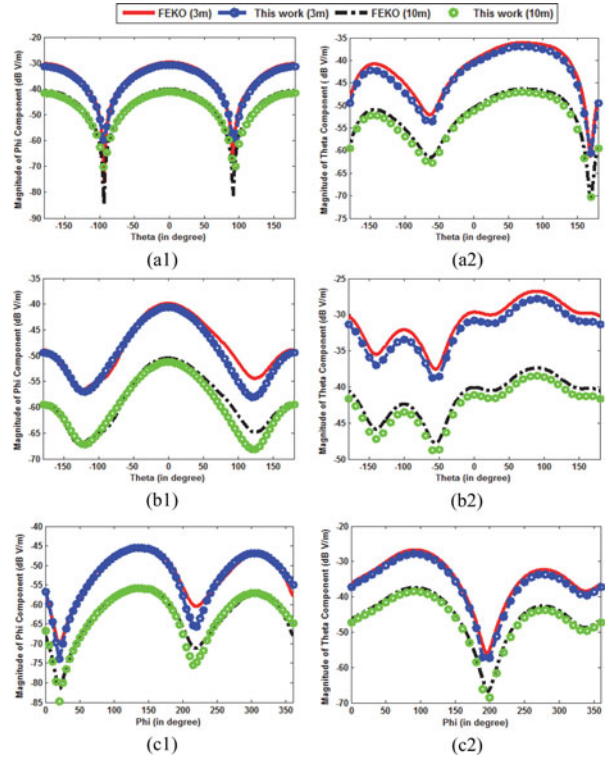

Fig. 14. Calculated electric fields at 3 and 10 m away. The left column are the ϕ-components, and the right column are the θ-components. (a1and a2) E-field in the xoz plane. (b1and b2) E-field in the yoz plane. (c1and c2) E-field in the xoy plane.
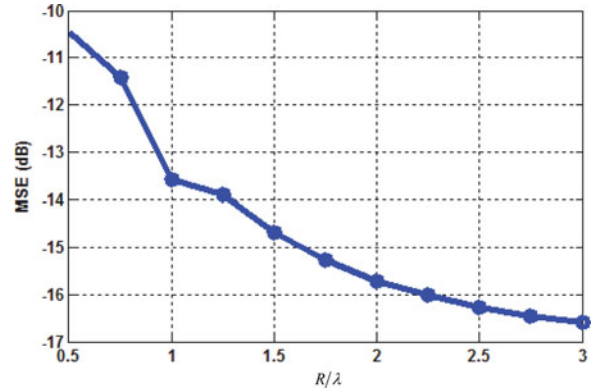

Fig. 15. Error function MSE (in dB) versus the distance (the radius of the sphere) for benchmark C.
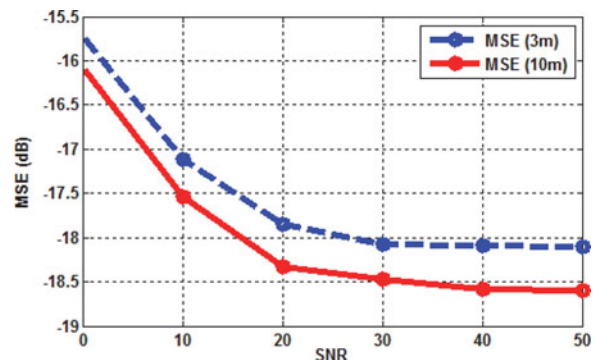

Fig. 16. Mean squared errors for various SNRs (in dB) when using the far field transformation technique proposed in this paper.

field has negligible influence on the FF, while the influence increases significantly when the SNR is smaller than 10 dB. This quantitative study provides a good reference for conducting NF measurements.

IV. CONCLUSION

A novel method based on the planar electric field sampling over slots is presented to model the radiated field from PCBs in closed shielding boxes with opening slots. The computation of complex DGF is avoided by the computation of the superposition of direct radiated field from the equivalent magnetic current and the scattered field by the induced electric current on the PEC box surface. The accuracy of the proposed two-step method is benchmarked for several PCB emission problems. The robustness of the algorithm is also investigated by adding random noise to the synthetic data. This method avoids the nonuniqueness of the conventional inverse methods and works for general complex radiators.

ACKNOWLEDGMENT

REFERENCES

[1] R. R. Tummala, "SOP: What is it and why: A new microsystem—integration technology paradigm-moore's law for system integration of miniatireized convergent systems of the next decade," *IEEE Trans. Adv. Packag.*, vol. 27, no. 2, pp. 241–249, May 2004.

[2] V. P. Kodali, *Engineering Electromagnetic Compatability*, 2nd ed. Piscataway, NJ, USA: IEEE Press, 2001.

[3] P. K. Saha and J. Dowling, "Reliable prediction of EM radiation from a PCB at the design stage of electronic equipment," *IEEE Trans. Electromagn. Compat.*, vol. 40, no. 2, pp. 166–174, May 1998.

[4] A. Ludwig, "Near-field far-field transformations using spherical wave expansions," *IEEE Trans. Antennas Propag.*, vol. 19, no. 2, pp. 214–220, Mar. 1971.

[5] W. M. Leach and D. T. Paris, "Probe compensated near-field measurements on a cylinder," *IEEE Trans. Antennas Propag.*, vol. 21, no. 4, pp. 435–445, Jul. 1973.

[6] J. J. H. Wang, "An examination of the theory and practices of planar near-field measurement," *IEEE Trans. Antennas Propag.*, vol. 36, no. 6, pp. 746–753, Jun. 1988.

[7] A. Taaghol and T. K. Sarkar, "Near-field to near/far-field trans- formation for arbitrary near-field geometry, utilizing an equivalent magnetic current," *IEEE Trans. Antennas Propag.*, vol. 38, no. 3, pp. 536–542, Aug. 1996.

[8] T. K. Sarkar and A. Taaghol, "Near-field to near/far-field transformation for arbitrary near-field geometry utilizing an equivalent electric current and MoM," *IEEE Trans. Antennas Propag.*, vol. 47, no. 3, pp. 566–573, Mar. 1999.

[9] J. L. A. Quijanoand and G. Vecchi, "Improved-accuracy source reconstruction on arbitrary 3-D surfaces," *IEEE Antennas Wireless Propaga. Lett.*, vol. 8, pp. 1046–1049, Sep. 2009.

[10] Y. Alvarez, F. Las-Heras, and M. R. Pino, "Reconstruction of equivalent currents distribution over arbitrary three-dimensional surfaces based on integral equation algorithms," *IEEE Trans. Antennas Propag.*, vol. 55, no. 12, pp. 3460–3468, Nov. 2007.

[11] T. Eibert and C. Schmidt, "Multilevel fast multipole accelerated inverse equivalent current method employing Rao–Wilton–Glisson discretization of electric and magnetic surface currents," *IEEE Trans. Antennas Propag.*, vol. 57, no. 4, pp. 737–746, Apr. 2009.

[12] J. R. Regue, M. Ribo, J. M. Garrell, and A. Martin, "A genetic algorithm based method for source identification and far-field radiated emissions prediction from near-field measurements for PCB characterization," *IEEE Trans. Electromagn. Compat.*, vol. 43, no. 4, pp. 520–530, Nov. 2001.

[13] X. Tong, D. W. P. Thomas, A. Nothofer, P. Sewell, and C. Christopoulos, "Modeling electromagnetic emissions from printed circuit boards in closed environments using equivalent dipoles," *IEEE Trans. Electromagn. Compat.*, vol. 52, no. 2, pp. 462–470, May 2010.

[14] Y. Alvarez, M. Rodriguez, F. Las-Heras, and M. M. Hernando, "On the use of the source reconstruction method for estimation radiated EMI in electronics circuits," *IEEE Trans. Inst. Meas.*, vol. 59, no. 12, pp. 3174–3183, Dec. 2010.

[15] S. R. Rengarajan and Y. Rahmat-Samii, "The field equivalence principle: Illustration of the establishment of the nonintuitive null fields," *IEEE Trans. Antennas Propog.*, vol. 42, no. 4, pp. 122–128, Aug. 2000.

[16] W. C. Chew, M. S. Tong, and B. Hu, *Integral Equations for Electromagmetic and Elastic Waves.* San Rafael, CA, USA: Morgan and Claypool Publisher, 2009.

[17] S. M. Rao, D. R. Wilton, and A. W. Glisson, "Electromagnetic scattering by surfaces of arbitrary shape," *IEEE Trans. Antennas Propag.*, vol. 30, no. 3, pp. 409–418, May 1982.

[18] J. Xiong, "Computation electromagnetics for microstrip and MEMS structures," Ph.D. dissertation, Dept. elect. comput. eng., Univ. of Illinois at Urbana-Champaign, USA, 2010.

[19] EM Software and Systems, FEKO Suite 6.0. [Online]. Available: http://www.feko.info

[20] J. A. Kong, *Electromagnetic Wave Theory.* Cambridge, MA, USA: EMW Publishing, 2008.

[21] J. L. Xiong, M. S. Tong, P. Atkins, and W. C. Chew, "Efficient evaluation of Casimir force in arbitrary three-dimensional geometries by integral equation methods," *Appl. Phys. Lett.*, vol. 374, no. 25, pp. 2517–2520, Jan. 2010.

[22] J. L. A. Quijano and G. Vecchi, "Near- and very near-field accuracy in 3-D source reconstruction," *IEEE Antennas Propag. Wireless Lett.*, vol. 9, pp. 634–637, Jun. 2010.
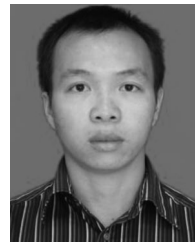
Ping Li (S'12) received the Bchelor's and the Master's degrees from the University of Electronic Science and Technology of China, Sichuan, China, in 2008 and 2010, respectively. Since 2010, he has been working toward the Ph.D. degreee with the center of Electromagnetics and Optics, the University of Hong Kong, Pok Fu Lam, Hong Kong.

His research interests include the inverse scattering/radiation problem, time domain discontinuous Galerkin finite element method and its application in microwave wave devices simulation, and nanophonotics analysis.

Mr. Li received the Engineering Postgraduate Fellowship from the Faculty of Engineering, the University of Hong Kong.

Li Jun Jiang (S'01–M'04–SM'13) received the B.S. degree in electrical engineering from the Beijing University of Aeronautics and Astronautics, Beijing, China, in 1993, the M.S. degree from the Tsinghua University, Beijing, in 1996, and the Ph.D degree from the University of Illinois at Urbana-Champaign, Urbana, USA, in 2004.

From 1996 to 1999, he was an Application Engineer with the Hewlett-Packard Company. He was a Postdoctoral Researcher, a Research Staff Member, and a Senior Engineer at IBM T. J. Watson Research Center. Since the end of 2009, he has been an Associate Professor with the Department of Electrical and Electronic Engineering, the University of Hong Kong, Pok Fu Lam, Hong Kong. His research interests includes electromagnetics, IC signal/power integrity, antennas, multidisciplinary EDA solutions, RF and microwave technologies, high performance computing (HPC), etc.

Dr. Jiang received the IEEE MTT Graduate Fellowship Award in 2003 and the Y. T. Lo Outstanding Research Award in 2004. He is an IEEE Antennas and Propagation Society (AP-S) member, and a Sigma Xi Associate member. He was the Semiconductor Research Cooperation Industrial Liaison for several academic projects. Since 2009, he has been the SRC Packaging High Frequency Topic TT Chair. He also serves as the Reviewer of the IEEE Transactions on several topics, and other primary electromagnetics and microwave related journals.